Available online at www.sciencedirect.com
ScienceDirect
Journal of the European Ceramic Society 30 (2010) 2741–2747
www.elsevier.com/locate/jeurceramsoc

Doping effect of divalent cations on sintering of polycrystalline yttria

Masayasu Kodo [a,*], Kohei Soga [a], Hidehiro Yoshida [b], Takahisa Yamamoto [c]

[a] Department of Materials Science and Technology, Tokyo University of Science, 2641 Yamazaki, Noda, Chiba 278-8510, Japan
[b] National Institute for Materials Science, 1-2-1 Sengen, Tsukuba, Ibaraki 305-0047, Japan
[c] Department of Advanced Materials Science, The University of Tokyo, 5-1-5 Kashiwanoha, Kashiwa, Chiba 277-8561, Japan

Received 23 November 2009; received in revised form 21 May 2010; accepted 29 May 2010
Available online 25 June 2010

Abstract

The sintering behavior of Y_2O_3 doped with 1 mol% of Ca^{2+}, Mg^{2+}, Mn^{2+}, Ni^{2+}, Sr^{2+} or Zn^{2+} was investigated by pressureless sintering in air at a sintering temperature in the range 900–1600 °C. The sintering temperature required for full densification in Y_2O_3 was reduced by 100–400 °C by the cation doping, while undoped Y_2O_3 was densified at 1600 °C. The most effective dopant among the examined cations was Zn^{2+}. The grain growth kinetics of undoped and cation-doped Y_2O_3 was described by the parabolic law. The grain boundary mobility of Y_2O_3 was accelerated by doping of the divalent cations. High-resolution transmission electron microscopy (HRTEM) observations and nano-probe X-ray energy dispersive spectroscopy (EDS) analyses confirmed that the dopant cations tended to segregate along the grain boundaries without forming amorphous layers. The improved sinterability of Y_2O_3 is probably related to the accelerated grain boundary diffusion owing to the grain boundary segregation of the dopant cations.

Keywords: Y_2O_3; Sintering; Grain boundaries; Transition metal oxides; Electron microscopy

1. Introduction

Y_2O_3 is receiving much attention not only as a refractory material, but also as a new component of dry-etching equipment because of its excellent corrosion resistance to halogen-family plasma.[1] Generally, high pressures (>40 MPa) and/or high temperatures (>1600 °C) under a reduced or hydrogen atmosphere have been used to obtain fully densified Y_2O_3 polycrystals.[2–9] Dutta and Gazza[4] obtained pore-free Y_2O_3 polycrystal by hot-press sintering at 1500 °C and under 40 MPa, Tsukuda and Muta[5] used hydrogen atmosphere sintering at 2240 °C, and Ikegami's group[8] fabricated pore-free Y_2O_3 polycrystal by vacuum sintering at 1600–1700 °C.

In contrast, the effects of sintering aids have been investigated for fabricating dense Y_2O_3 by pressureless sintering in air. It has been reported that the sintering temperature of Y_2O_3 can be reduced by doping with a divalent alkaline metal cation. For instance, the sintering temperature of Y_2O_3 to achieve the relative density of 90% was reduced from 1700 to 1500 °C by doping with 1 mol% Mg^{2+} or Ca^{2+} under pressureless sintering in air.[10] Analysis of the densification rate during two-step sintering in Y_2O_3 doped with 1 mol% Mg^{2+} or Nb^{5+} at a sintering temperature of 1000–1300 °C revealed that the grain boundary diffusivity in Y_2O_3 was accelerated by Mg^{2+} doping, but decelerated by Nb^{5+} doping.[11] More recently, our group examined the doping effect of 1 mol% Ni^{2+} or Mn^{2+} on the sinterability of 1 mol% Er^{3+}-doped Y_2O_3[12] and found that the sinterability of Er^{3+}-doped Y_2O_3 was highly improved by Ni^{2+} or Mn^{2+} doping. In addition, the grain growth kinetics of dense and single-phase Y_2O_3 with or without dopant (Mg, Sr, Sc, Yb, Gd, La, Ti, Zr, Ce and Nb) has been investigated[13] in air and in a reduced atmosphere at temperatures between 1500 and 1650 °C. The previous study[13] demonstrated that the grain growth behavior of dense and single-phase Y_2O_3 with a grain size of 0.3–12.5 μm was described by the parabolic law:

$$d^2 - d_0^2 = 2M\gamma(t - t_0), \quad (1)$$

where d_0 is the reference grain size at time t_0, d the average grain size at time t, γ the grain boundary energy, and M is the grain boundary mobility. Analysis of the grain growth kinetics revealed that the grain boundary mobility of Y_2O_3

* Corresponding author. Tel.: +81 4 7124 9689; fax: +81 4 7124 1526.
E-mail address: kodo@sogalabo.jp (M. Kodo).

0955-2219/$ – see front matter © 2010 Elsevier Ltd. All rights reserved.
doi:10.1016/j.jeurceramsoc.2010.05.028

Table 1
Sintering conditions of the samples for grain growth experiments.

Sample	Undoped Y_2O_3	+1 mol% Mn	+1 mol% Sr	+1 mol% Zn
Sintering temp. (°C)	1700	1330	1605	1280
Sintering time (h)	2	1	1.5	2

was controlled by a cation interstitial mechanism, and was enhanced/suppressed by doping of accepter/donor dopants.

Previous studies concerning sintering aids suggest that doping of divalent cations enhances matter transport (and consequently densification during sintering) in Y_2O_3. This study aims to investigate the effect of divalent cation doping on the sinterability of Y_2O_3. In addition, grain growth experiments were performed for undoped and cation-doped Y_2O_3 in order to clarify the doping effect on the grain boundary mobility of Y_2O_3.

2. Experimental procedure

The samples used in this study were undoped Y_2O_3 and 1 mol% Ca^{2+}-, Mg^{2+}-, Mn^{2+}-, Ni^{2+}-, Sr^{2+}- or Zn^{2+}-doped Y_2O_3. The starting powder was commercially available Y_2O_3 powder with a purity of 99.9% and an average grain size of 20 nm (BB-type; Shin-Etsu Chemical Co., Ltd., Japan). $Ca(CH_3COO)_2{\cdot}H_2O$ (99.0%, Kanto Chemical Co., Ltd., Japan), $Mg(CH_3COO)_2{\cdot}4H_2O$ (99.3%, Kanto Chemical Co., Ltd., Japan), $Mn(CH_3COO)_2{\cdot}4H_2O$ (99%, Kanto Chemical Co., Ltd., Japan), $Ni(CH_3COO)_2{\cdot}4H_2O$ (98%, Kanto Chemical Co., Ltd., Japan), $Sr(CH_3COO)_2{\cdot}1/2H_2O$ (99.0%, Kanto Chemical Co., Ltd., Japan) and $Zn(CH_3COO)_2$ (99.99%, Aldrich) were used as dopant sources. The Y_2O_3 powder with a dopant source was ball-milled with TZP balls in ethanol for 24 h, dried and then sifted through a 60-mesh sieve for granulation without any binders. Green bodies were prepared by cold isostatic pressing under 120 MPa following uniaxial compression at approximately 20 MPa. The green bodies were sintered at temperatures between 900 and 1600 °C for 3 h in air with a heating rate of 300 °C/h. The density of the sintered bodies was measured by the Archimedes method. Relative density was estimated as a ratio of the actual density to the theoretical density of 5.03 g/cm^3, the value of which is the theoretical density in pure Y_2O_3 at room temperature.[14] The theoretical density in cation-doped Y_2O_3 is 5.00–5.04 g/cm^3 when 1 mol% of the dopant cations are either soluble or insoluble in Y_2O_3.

Conventional grain growth experiments were performed in undoped, Mn^{2+}-, Sr^{2+}- and Zn^{2+}-doped Y_2O_3 in order to measure the grain boundary mobility of the present materials. The green bodies CIPed at 120 MPa were sintered in air under conditions shown in Table 1 to obtain a relative density of more than 99%. The sintered samples were then annealed at 1380–1700 °C for 1–36 h in air with a heating rate of 10 °C/min.

The microstructure of the sintered samples was observed using a scanning electron microscope (SEM; S-4200, Hitachi, Japan). In samples with low densities (relative density <80%), the average grain size of the sintered samples was estimated using an average diameter of grains on the fracture surface. In samples with high densities (relative density >80%), the average grain size was obtained by multiplying an average linear intercept length by 1.57[15] on the polished and thermally etched surface. High-resolution transmission electron microscopy (HRTEM; EM-002BF, Topcon, Japan) observations were also performed for the detailed analysis of grain boundaries in the sintered samples. Chemical analysis in the vicinity of grain boundaries was carried out with an X-ray energy dispersive spectrometer (EDS; Voyager, Noran Instruments Inc., U.S.A.) equipped to the HRTEM using a probe size of about 1 nm.

3. Results and discussion

Fig. 1 shows the relative density of sintered samples as a function of sintering temperature. In undoped Y_2O_3, slight densification takes place below the sintering temperature of 1100 °C, and the relative density of 97% is barely achieved at 1600 °C. In contrast, densification in Zn^{2+}-, Ni^{2+}- or Mn^{2+}-doped Y_2O_3 takes place rapidly even at 1100 °C. At the sintering temperature of 1200 °C, the relative density of 99%, 96%, 95% and 72% is already achieved in Zn^{2+}-, Ni^{2+}-, Mn^{2+}- and Mg^{2+}-doped Y_2O_3, respectively, whereas the relative density in undoped Y_2O_3 is still 58%. The doping of Ca^{2+} or Sr^{2+} suppresses the densification of Y_2O_3 below 1300 or 1500 °C, respectively, but facilitates densification at relatively high temperatures. All the dopant cations essentially reduce the sintering temperature of Y_2O_3. Among the dopant cations examined, Zn^{2+}

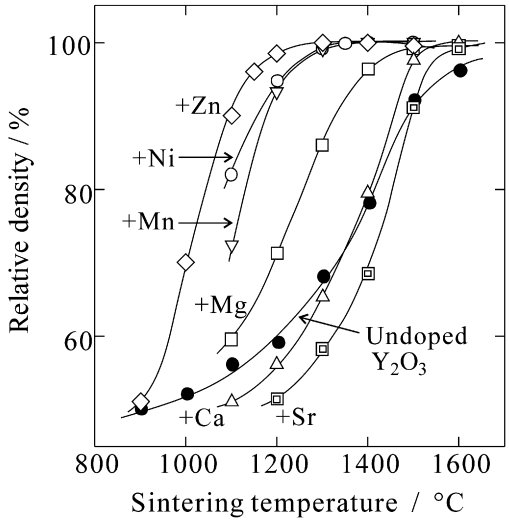

Fig. 1. Relative density of undoped and cation-doped Y_2O_3 as a function of sintering temperature. ◊ 1 mol% Zn^{2+}-doped Y_2O_3; ◯ 1 mol% Ni^{2+}-doped Y_2O_3; ▽ 1 mol% Mn^{2+}-doped Y_2O_3; □ 1 mol% Mg^{2+}-doped Y_2O_3; △ 1 mol% Ca^{2+}-doped Y_2O_3; ⊡ 1 mol% Sr^{2+}-doped Y_2O_3; ● undoped Y_2O_3.

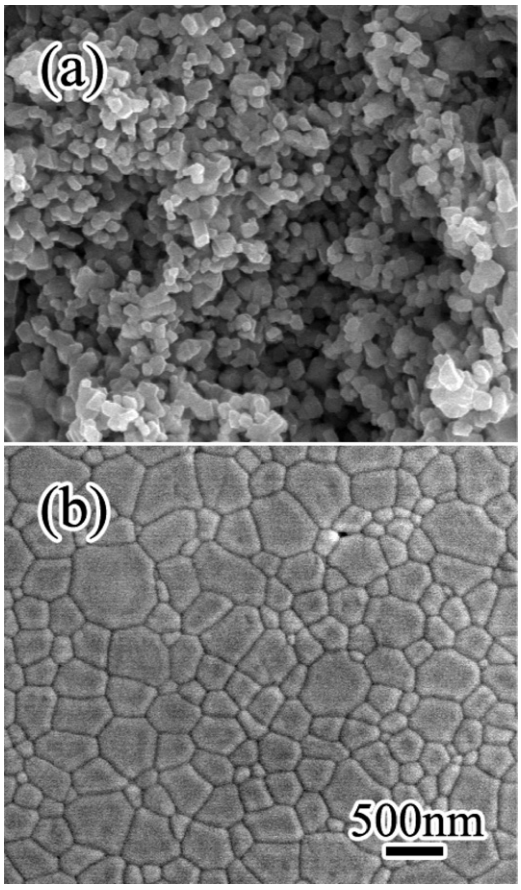

Fig. 2. SEM micrographs of (a) undoped and (b) Zn^{2+}-doped Y_2O_3 sintered at 1200 °C.

is the most effective dopant in improving the sinterability of Y_2O_3; the sintering temperature in Zn^{2+}-doped Y_2O_3 required for full densification is 1200 °C, which is 400 °C lower than that required for undoped Y_2O_3.

Fig. 2 shows SEM micrographs of a (a) fracture surface of undoped Y_2O_3 and (b) thermally etched surface of Zn^{2+}-doped Y_2O_3 sintered at 1200 °C. The undoped Y_2O_3 sintered at 1200 °C still exhibits a porous structure with limited grain growth. In contrast, the Zn^{2+}-doped sample exhibits an almost pore-free microstructure that consists of uniform and equiaxed grains without extremely large grains relative to matrix grains. Doping with Zn^{2+} allows fabrication of a dense, fine-grained Y_2O_3 polycrystal at low temperatures.

Fig. 3 shows SEM images of undoped and cation-doped Y_2O_3, which exhibit a relative density of more than 97%. The sintering temperatures are the lowest necessary to reach the relative density for each sample, and are indicated in the figure caption. All the images exhibit a single-phase, uniform and equiaxed grain structure without extremely large grains relative to matrix grains. Pores are located at the multiple junctions in the present materials. Mg^{2+}-doped Y_2O_3 sintered at 1400 °C (Fig. 3c) shows a single-phase structure, but secondary-phase particles with dark contrast are observed in Mg^{2+}-doped Y_2O_3 sintered at 1500 and 1600 °C. According to the phase diagram of a Y_2O_3–MgO system,[16] the solubility of MgO in Y_2O_3 is less than 1 mol% at 1600 °C and no intermediate compound is observed. TEM–EDS analysis of the secondary-phase particles in the Mg^{2+}-doped sample sintered at 1500 °C confirms only Mg and O, but not Y. The secondary-phase particles in Mg^{2+}-doped Y_2O_3 sintered above 1500 °C must be MgO. Fig. 4 shows the average grain size of Y_2O_3 grains in sintered samples with a relative density of more than 90% as a function of sintering temperature. The average grain size of the cation-doped samples excepting Mg^{2+}-doped Y_2O_3 sintered above 1500 °C is larger than that of undoped Y_2O_3, even though the effect of pores on the grain growth is not negligible at the relative density of 90%. In Mg^{2+}-doped Y_2O_3 sintered above 1500 °C, the average grain size is nearly the same as that of undoped Y_2O_3. This is probably due to the precipitation of secondary-phase particles. The average grain size of Y_2O_3 is essentially increased by the cation doping. The increased average grain size owing to the cation doping suggests an acceleration of the grain boundary migration rate.

Fig. 5 shows a plot of $d^2 - d_0^2$ as a function of $t - t_0$ in Y_2O_3 doped with Mn^{2+}, Sr^{2+} or Zn^{2+} at 1480 °C. SEM observations revealed that the annealed samples exhibited a single-phase material with a grain size in the range 0.8–5 μm. The grain growth behavior of the present samples can be described by the parabolic law (Eq. (1)). From the slope of the straight lines in Fig. 5, the grain boundary mobilities can be calculated by using a γ value of 0.3 J/m^2.[13] The calculated grain boundary mobilities are shown in Fig. 6. Previous data for undoped and Sr^{2+}-doped Y_2O_3[13] is also plotted for comparison. The mobility data of undoped and Sr^{2+}-doped Y_2O_3 in this study is on the straight lines extrapolated from the reported data of undoped and Sr^{2+}-doped Y_2O_3, respectively. The present mobility data of undoped and Sr^{2+}-doped Y_2O_3 is consistent with the reported data. A comparison of the grain boundary mobilities of undoped and Mn^{2+}, Sr^{2+} or Zn^{2+}-doped Y_2O_3 shows that the grain boundary mobility is increased by the cation doping. The increased grain boundary mobility indicates that the grain boundary and/or lattice diffusion is enhanced by the doping. Although the rate-controlling diffusion pass of densification of Y_2O_3 cannot be clarified at present, the accelerated grain boundary mobility is consistent with the improved sinterability of Y_2O_3 owing to the enhanced diffusion by the doping. The doped cations presumably play a key role in accelerating diffusion of Y_2O_3.

In order to verify the role of the dopant cations, the distribution of the doped cations was investigated by HRTEM–EDS analysis. Fig. 7(a) shows a HRTEM image of a triple junction in Zn^{2+}-doped Y_2O_3 sintered at 1300 °C. Lattice fringes for the three grains can be clearly seen in the HRTEM image, and neither a secondary-phase nor amorphous layer is observed at the grain boundaries and the triple junction. The microstructural observation indicates that Zn^{2+}-doped Y_2O_3 is a single-phase material. Fig. 7(b) and (c) shows nano-probe EDS spectra taken from the grain boundary and the grain interior (5 nm off the grain boundary), respectively. The analyzed areas are indicated in Fig. 7(a) by black circles. The enlarged spectra for characteristic X-ray energy in the range 7–10 keV are inserted in Fig. 7(b) and (c). The peaks assigned to Cu at 8.1 and 8.9 keV originate from the specimen holder. The peaks from Zn are observed in the spectrum taken from the grain boundary, but are not observed in the

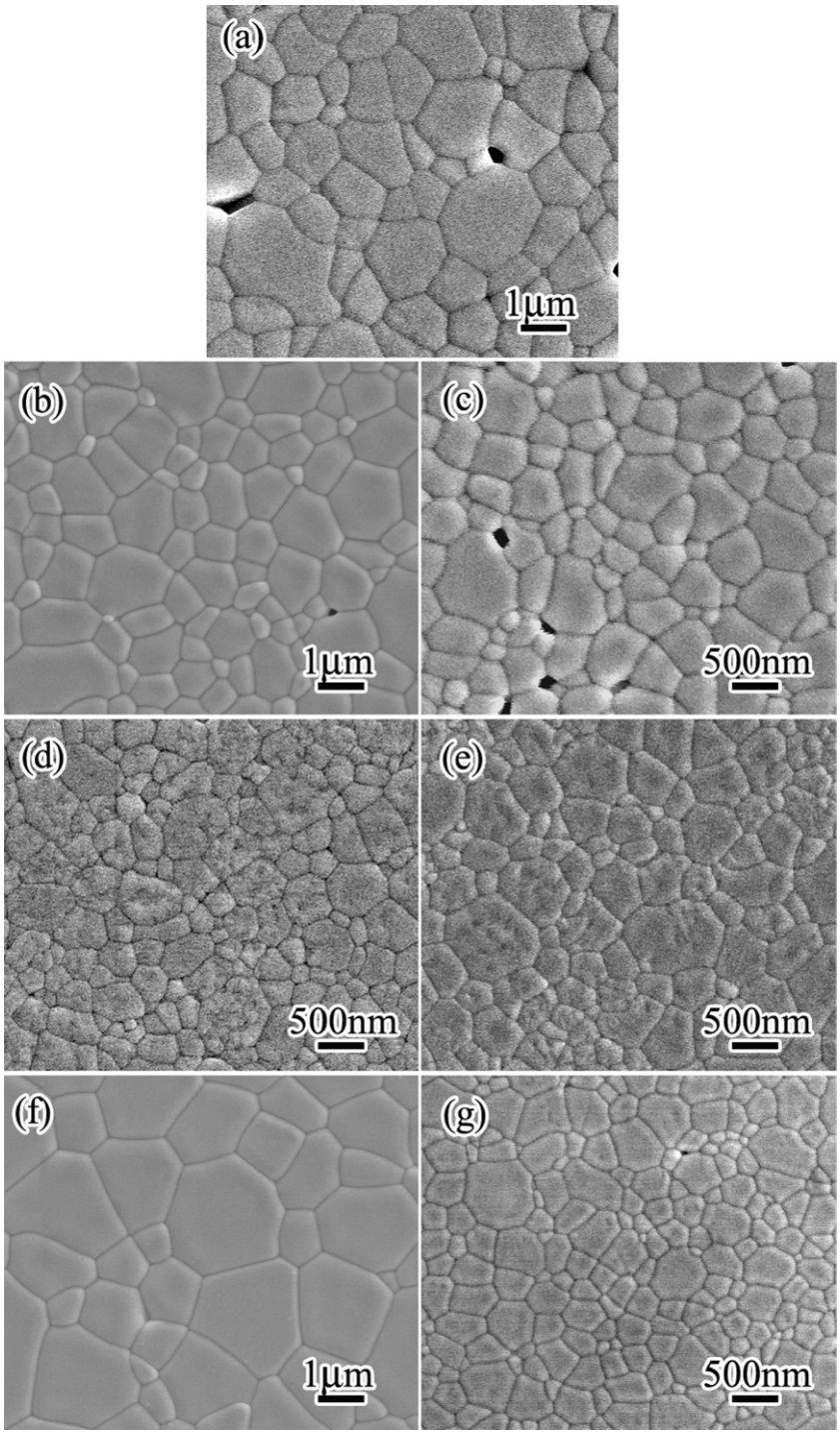

Fig. 3. SEM micrographs of (a) undoped Y_2O_3 sintered at 1600 °C, (b) Ca^{2+}-doped Y_2O_3 sintered at 1500 °C, (c) Mg^{2+}-doped Y_2O_3 sintered at 1400 °C, (d) Mn^{2+}-doped Y_2O_3 sintered at 1300 °C, (e) Ni^{2+}-doped Y_2O_3 sintered at 1300 °C, (f) Sr^{2+}-doped Y_2O_3 sintered at 1600 °C, and (g) Zn^{2+}-doped Y_2O_3 sintered at 1200 °C.

spectrum from the grain interior. These results indicate that the doped Zn^{2+} cation tends to segregate in the vicinity of the grain boundaries without forming second phases. Nano-probe EDS analysis of the other cation-doped Y_2O_3 samples examined in this study also revealed that the doped cations segregate in the vicinity of the grain boundaries as observed for Zn^{2+}. The grain boundary segregation of the doped cations must be the origin of the doping effect on sintering of Y_2O_3; the segregated dopant cations must enhance the grain boundary diffusion, and hence the sinterability of Y_2O_3 is facilitated by the doping.

It has been shown that doping with Mg^{2+} accelerates grain boundary diffusivity[11] and grain growth of Y_2O_3.[13] The previous studies concluded that the accelerated diffusivity and mobility owing to Mg^{2+} doping were attributed to the formation of oxygen vacancies, and substitution of the divalent cation at a Y^{3+} site should induce the oxygen vacancy in order to maintain

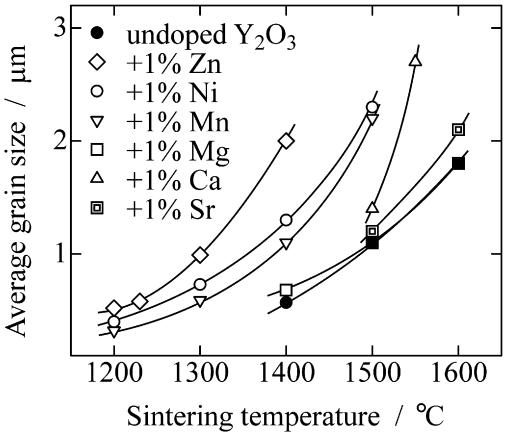

Fig. 4. Average grain size of undoped and cation-doped Y_2O_3 as a function of sintering temperature. ◊ 1 mol% Zn^{2+}-doped Y_2O_3; ○ 1 mol% Ni^{2+}-doped Y_2O_3; ▽ 1 mol% Mn^{2+}-doped Y_2O_3; □ 1 mol% Mg^{2+}-doped Y_2O_3; △ 1 mol% Ca^{2+}-doped Y_2O_3; ⊡ 1 mol% Sr^{2+}-doped Y_2O_3; ● undoped Y_2O_3.

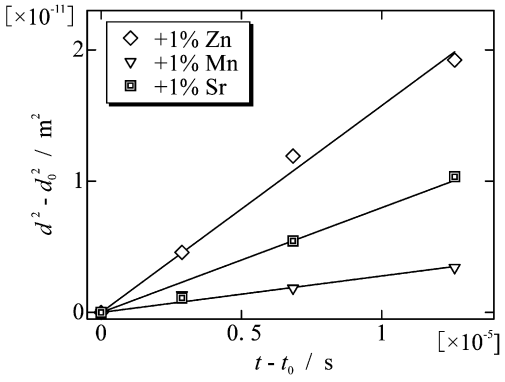

Fig. 5. Grain growth behavior of undoped and cation-doped Y_2O_3 at 1480 °C. ◊ 1 mol% Zn^{2+}-doped Y_2O_3; ▽ 1 mol% Mn^{2+}-doped Y_2O_3; ⊡ 1 mol% Sr^{2+}-doped Y_2O_3.

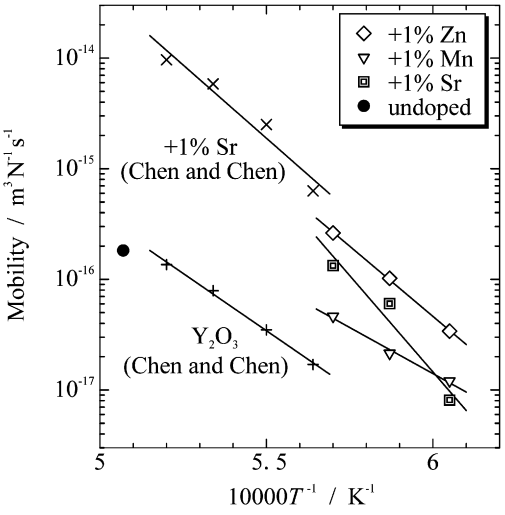

Fig. 6. Grain boundary mobility in undoped and cation-doped Y_2O_3. ◊ 1 mol% Zn^{2+}-doped Y_2O_3; ▽ 1 mol% Mn^{2+}-doped Y_2O_3; ⊡ 1 mol% Sr^{2+}-doped Y_2O_3; ● undoped Y_2O_3; × 1 mol% Sr^{2+}-doped Y_2O_3 (reported data); + undoped Y_2O_3 (reported data).

electronic neutrality in Y_2O_3.[13] In Y_2O_3 doped with divalent cations (M^{2+}), oxygen vacancies are introduced by the following reaction:

$$MO \rightarrow M'_Y + \frac{1}{2}V_O^{\bullet\bullet} + O_O * . \quad (2)$$

In the present study, the segregated divalent cations must involve the formation of oxygen anion vacancies as described by Eq. (2) in the vicinity of the grain boundaries, and accordingly accelerate the grain boundary diffusion of Y_2O_3.

It should be noted that the doping effect on sintering depends on the type of dopant. The origin of the doping effect cannot be explained solely from the formation of vacancies. The doping effect is thought to be affected by lattice distortion; substitution of cations, which have a smaller ionic radius, at a Y^{3+} site will

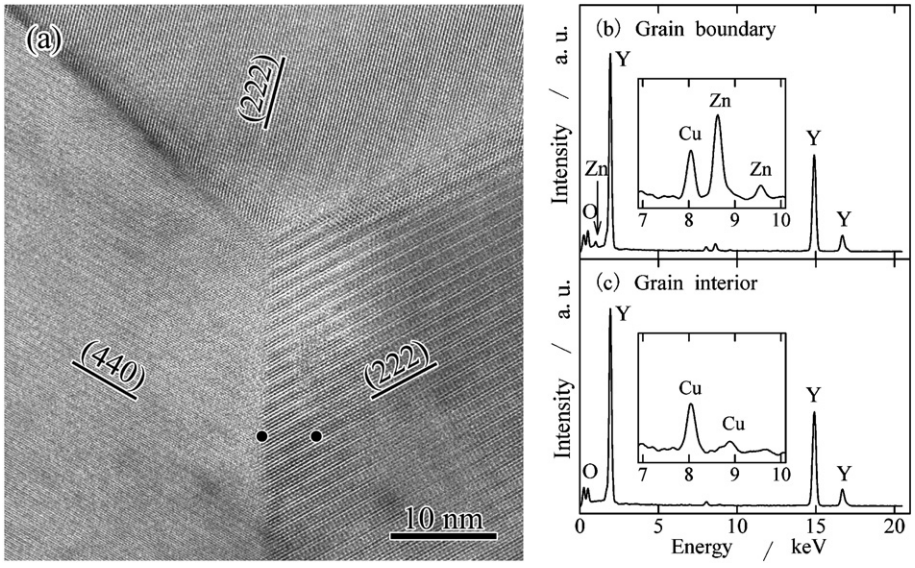

Fig. 7. (a) HRTEM image of a triple junction in Zn^{2+}-doped Y_2O_3 sintered at 1300 °C, (b) EDS spectra measured at the grain boundary, and (c) the grain interior with a probe size of about 1 nm. The analyzed areas are indicated in (a).

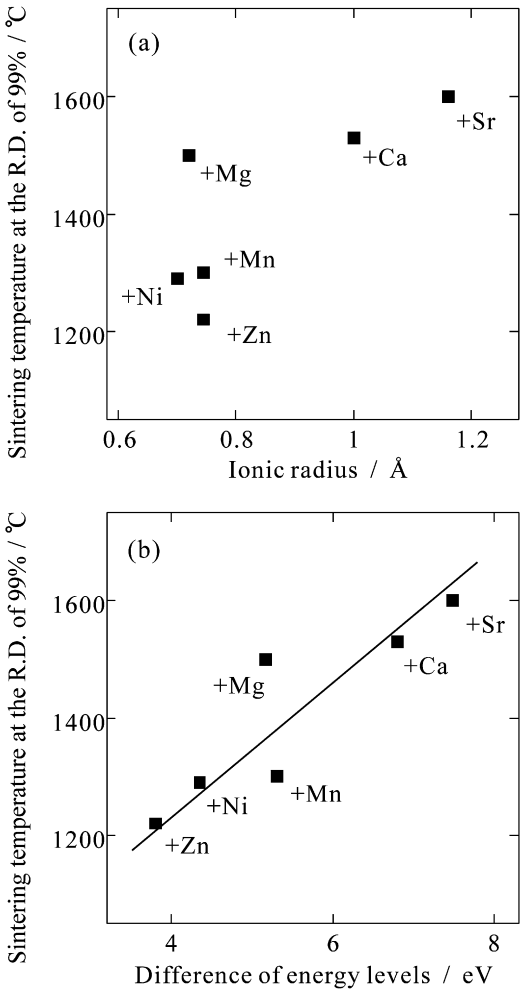

Fig. 8. Sintering temperature required for a relative density of 99% as a function of (a) ionic radius of cations and (b) difference in energy levels between the O 2p orbital and an outer-shell orbital of a metal.

expand the interatomic distance of Y–O, and atomic diffusion is accordingly expected to be enhanced. The magnitude of the grain boundary diffusivity in cation-doped Y_2O_3 can be roughly estimated by the sintering temperature required for a relative density of 99%. Fig. 8(a) shows a plot of sintering temperature required for a relative density of 99% as a function of the ionic radius[17] of the dopant cations with the coordination number of 6. In Y_2O_3 doped with Sr^{2+}, Ca^{2+} or Mg^{2+}, the sintering temperature decreases with decreasing ionic radius. In Y_2O_3 doped with Mn^{2+}, Ni^{2+} or Zn^{2+} (transition metal elements), the sintering temperature is 1200–1300 °C. In spite of nearly the same ionic size of Mg^{2+} and the transition metal ions, the sintering temperature in Y_2O_3 doped with a transition metal ion is significantly lower than that of Mg^{2+}-doped Y_2O_3. Therefore, the doping effect on the sinterability of Y_2O_3 cannot be explained solely from the ionic radius. Recent studies on the sintering of oxide ceramics such as Al_2O_3[18,19] and TZP[20,21] have pointed out that the ionicity of the oxygen anion in the grain boundaries segregated with the dopant cations correlates closely with atomic diffusion. When the ionic charge of the oxygen anion is decreased by dopant cations, the ionic bond between anion and cation is weakened, and atomic diffusion is accordingly enhanced. In the present materials, the decrement of the ionicity around O^{2-} in the grain boundaries may accelerate the grain boundary diffusion of Y^{3+}. The ionicity can be roughly expressed by the difference of energy levels between the O 2p orbital and an outer-shell orbital of a metal.[22] Fig. 8(b) shows a plot of sintering temperature required for a relative density of 99% as a function of the difference in energy levels.[23] The sintering temperature decreases with a decrease in the difference of energy levels. It should be noted that the correlation in Fig. 8(b) is better than that shown in Fig. 8(a). The doping effect on the sinterability of Y_2O_3 is probably related not only to the ionic valence of the dopant cations, but also to ionicity in the vicinity of the grain boundaries.

4. Conclusions

The sintering temperature of Y_2O_3 required for full densification was reduced by 100–400 °C by doping with divalent cations at a doping content of 1 mol%. Among the investigated cations, Zn^{2+} was the most effective dopant in improving the sinterability of Y_2O_3. The parabolic grain growth was observed in dense, undoped and cation-doped Y_2O_3. The grain boundary mobility was enhanced by doping of the divalent cations. HRTEM observations and nano-probe EDS analyses revealed that cation-doped Y_2O_3 was composed of single-phase materials and that the doped cations tended to segregate along the grain boundaries. The accelerated grain boundary mobility suggests an enhancement of lattice and/or grain boundary diffusion, which is consistent with the improved sinterability of Y_2O_3. Because of the dopant segregation along the grain boundaries, enhanced grain boundary diffusion is likely to attribute to the improved sinterability of Y_2O_3.

Acknowledgements

This work was financially supported by an “Academic Frontier” Project for Private Universities (2006–2010), a Grant-in-Aid for Encouragement of Young Scientists (A)-19686042 from the Ministry of Education, Culture, Sports and Technology of Japan (MEXT), and a Grant-in-Aid for Scientific Research on Priority Areas “Nano Materials Science for Atomic-scale Modification 474” from MEXT.

References

1. Iwasawa J, Nishimizu R, Tokita M, Kiyohara M, Uematsu K. Plasma-resistant dense yttrium oxide film prepared by aerosol deposition process. *J Am Ceram Soc* 2007;**90**:2327–32.
2. Lefever RA, Matsko J. Transparent yttrium oxide ceramics. *Mater Res Bull* 1967;**2**:865–9.
3. Majima K, Niimi N, Watanabe M, Katsuyama S, Nagai H. Effect of LiF addition on the preparation of transparent Y_2O_3 by the vacuum hot pressing method. *J Alloys Compd* 1993;**193**:280–2.
4. Dutta SK, Gazza GE. Transparent Y_2O_3 by hot-pressing. *Mater Res Bull* 1969;**4**:791–6.
5. Tsukuda Y, Muta A. Sintering of Y_2O_3 at high temperatures. *J Ceram Soc Jpn* 1976;**84**:585–9.

6. Jorgensen PJ, Anderson RC. Grain-boundary segregation and final-stage sintering of Y_2O_3. *J Am Ceram Soc* 1967;**50**:553–8.
7. Grescovich C, Woos KN. Fabrication of transparent ThO_2-doped Y_2O_3. *Ceram Bull* 1973;**52**:473–8.
8. Saito N, Matsuda S, Ikegami T. Fabrication of transparent yttria ceramics at low temperature using carbonate-derived powder. *J Am Ceram Soc* 1998;**81**:2023–8.
9. Ikegami T, Li J-G, Mori T, Moriyoshi Y. Fabrication of transparent yttria ceramics by the low-temperature synthesis of yttrium hydroxide. *J Am Ceram Soc* 2002;**85**:1725–9.
10. Katayama K, Osawa H, Akiba T, Urabe K, Yanagida H. Sintering of yttrias with addition of divalent metal oxide and water vapor pressure dependence of their electrical conductivity. *J Mater Sci* 1990;**25**:1503–8.
11. Wang X-H, Chen P-L, Chen I-W. Two-step sintering of ceramics with constant grain-size. I. Y_2O_3. *J Am Ceram Soc* 2006;**89**:431–7.
12. Kodo M, Soga K, Yoshida H, Yamamoto T. Low temperature sintering of polycrystalline yttria by transition metal ion doping. *J Ceram Soc Jpn* 2009;**117**:765–8.
13. Chen P-L, Chen I-W. Grain boundary mobility in Y_2O_3: defect mechanism and dopant effect. *J Am Ceram Soc* 1996;**79**:1801–9.
14. Smrcok L. Rietveld refinement of Y_2O_3 using the Pearson VII profile shape function. *Crystal Res Technol* 1989;**24**:607–11.
15. Fullman RL. Measurement of particle sizes in opaque bodies. *Trans AIME* 1953;**197**:447–52.
16. Tresvyatskii SG, Lopato LM, Ogorodnikova AA, Shevchenko AV. Phase diagrams of the system formed by yttrium erbium, and ytterbium oxides with magnesium oxide. *Inorg Mater (Engl Transl)* 1971;**7**:1798–801.
17. Shannon RD, Prewitt CT. Effective ionic radii oxide and fluorides. *Acta Crystrallogr Sect B: Struct Sci* 1969;**25**:925–46.
18. Yoshida H, Ikuhara Y, Sakuma T. Grain boundary electronic structure related to the high-temperature creep resistance in polycrystalline Al_2O_3. *Acta Mater* 2002;**50**:2955–66.
19. Yoshida H, Hashimoto S, Yamamoto T. Dopant effect on grain boundary diffusivity in polycrystalline alumina. *Acta Mater* 2005;**53**:433–40.
20. Kuwabara A, Nakano M, Yoshida H, Ikuhara Y, Sakuma T. Superplastic flow stress and electronic structure in yttria-stabilized tetragonal zirconia polycrystals doped with GeO_2 and TiO_2. *Acta Mater* 2004;**52**:5563–9.
21. Sakuma T, Yoshida H. High temperature grain boundary plasticity in ceramics. *Mater Trans* 2009;**50**:229–35.
22. Harrison WA. *Electronic Structure and the Properties of Solids*. New York: Dover Publications Inc.; 1980. p. 20.
23. Herman F, Skillman S. *Atomic Structure Calculations*. New Jersey: Prentice-Hall; 1963. p. 3.